Applicability of regular particle shapes in light scattering calculations for atmospheric ice particles

Andreas Macke and Michael I. Mishchenko

We ascertain the usefulness of simple ice particle geometries for modeling the intensity distribution of light scattering by atmospheric ice particles. To this end, similarities and differences in light scattering by axis-equivalent, regular and distorted hexagonal cylindric, ellipsoidal, and circular cylindric ice particles are reported. All the results pertain to particles with sizes much larger than a wavelength and are based on a geometrical optics approximation. At a nonabsorbing wavelength of 0.55 μm, ellipsoids (circular cylinders) have a much (slightly) larger asymmetry parameter g than regular hexagonal cylinders. However, our computations show that only random distortion of the crystal shape leads to a closer agreement with g values as small as 0.7 as derived from some remote-sensing data analysis. This may suggest that scattering by regular particle shapes is not necessarily representative of real atmospheric ice crystals at nonabsorbing wavelengths. On the other hand, if real ice particles happen to be hexagonal, they may be approximated by circular cylinders at absorbing wavelengths.

1. Introduction

The major problem in modeling the solar radiative properties of cirrus clouds is the nonsphericity of atmospheric ice crystals that prevents efficient analytical treatment of their single scattering properties. Fortunately, the majority of ice particles are considerably larger than the wavelengths of the incoming solar radiation, especially in the visible spectral region. Therefore, the geometrical optics approximation offers a conceptually simple although time-consuming way to simulate single scattering by almost arbitrarily shaped scatterers.[1–5] Whereas these papers take more and more complex particle geometries such as bullet rosettes, dendrites, or polycrystals into account, in this paper we examine the possibility of representing the scattering properties of atmospheric ice crystals by simple ellipsoidal and circular cylindrical geometries. One advantage is that ray-tracing computations for simple geometries are much faster than for polyhedral crystal shapes that accelerate averaging over particle sizes and eccentricities or multispectral calculations. On the other hand, the three (two) semiaxes of an ellipsoid (circular cylinder) allow for a variability of particle shapes that may cover to some extent the natural variability of atmospheric ice crystal habits.

Another motivation arises from uncertainties in our knowledge of real ice particle shapes. The study of observationally derived two-dimensional ice crystal shadow images[6] or replicas[7,8] clearly demonstrates that solid hexagonal columns or plates are a strong idealization of atmospheric ice crystals. However, statistically reliable shape information is difficult to extract from these data, partly because of the strong natural variability. Therefore it appears reasonable to ascertain the use of nonhexagonal but still simple geometries as substitutes for a polydispersion of complicated ice particle shapes.

Because of the lack of sharp edges, ellipsoids do not provide strong halos that are characteristic of regular hexagonal particles. However, the absence of these features, as reported in a number of radiance measurements in or above cirrus clouds,[9,10] emphasizes the potential use of nonhexagonal par-

The authors are with the NASA Goddard Institute for Space Studies, 2880 Broadway, New York, New York 10025. A. Macke is also with the Department of Applied Physics, Columbia University, 2880 Broadway, New York, New York 10025. M. I. Mishchenko is also with the Institute of Terrestrial and Planetary Atmospheres, State University of New York at Stony Brook, Stony Brook, New York 11794.

Received 28 August 1995; revised manuscript received 29 January 1996.

0003-6935/96/214291-06$10.00/0

ticle shapes. A circular cylinder basically shows the 46° halo that is due to a minimum deviation at 90° ice prisms. However, the magnitude of this halo component is extremely weak. Furthermore, melting processes at warmer altitude levels of cirrus clouds or at levels at which mixed phases occur may result in smooth particle boundary surfaces, which may be better approximated by ellipsoids or circular cylinders than by sharp-edged hexagonal particles.

Recent studies of solar reflectivities[11,12] show that an agreement between measurements and model results requires an asymmetry parameter [see Eq. (2)] as small as 0.7. Hexagonal particles, on the other hand, provide values around 0.8 and larger. Therefore, it is interesting to see how other simple particle shapes compare with these values.

The **T**-matrix method[13] allows for exact solutions of scattering by randomly oriented rotational symmetric particles[14] with size parameters as high as 100.[15] At infrared wavelengths for which geometrical optics is not always an acceptable approximation, especially for smaller ice crystals, our results may give some indications regarding the most promising particle shape for future **T**-matrix applications.

We are aware that atmospheric ice particles are neither ellipsoidal nor circular cylindric. However, for the reasons pointed out above in this paper we ascertain the possibility of approximating light scattering on real ice particles by these simple geometries. Based on the observationally derived indications stated above, a certain particle shape can be regarded as a good approximation if its scattering properties are more isotropic than those of hexagonal cylinders. A discussion of light scattering by ellipsoids and circular cylinders may be interesting in its own right. The origins of the most important scattering features are explained in Sections 3 and 4. However, our major focus in this paper is a comparison between different particle shapes. A more detailed investigation of light scattering by these simple geometries including the full phase matrix will be a subject of future research.

In Section 2 we describe the ray-tracing model and the geometry of the particles used in this study. Comparisons between the scattering properties of nonabsorbing aspect-ratio-equivalent hexagonal cylinders, ellipsoids, and circular cylinders are shown in Section 3. In Section 4 we investigate to what extent absorption affects the scattering features of the individual particle types. For simplicity we focus on the most important photometric characteristics of light scattering, i.e., the scattering phase function and related quantities. Other phase matrix elements are not discussed. Given the high accuracy of the scalar approximation in solving the radiative transfer equation,[16] this is fully justified unless polarimetric remote sensing is concerned. The latter requires close consideration of the true particle shapes since polarization features are known to be extremely shape dependent for moderate to large particle sizes.[17,5] Therefore, note that the similarities and differences in the scattering phase function discussed below may not hold for the remaining phase matrix elements.

2. Ray-Tracing Model and Particle Geometry

The present ray-tracing model is basically identical to the one described in Ref. 5 in which the next point of intersection of a light ray with a polyhedral crystal surface can be determined by applying a search algorithm along all the individual crystal facets. Since this procedure has to be carried out after each reflection or refraction event, computation time increases strongly with an increasing number of facets defining the particle. On the other hand, the next point of intersection of a light ray with an ellipsoid surface can be calculated directly from the ellipsoid semiaxes and the location of the light ray. For circular cylinders, the search algorithm has to be performed for the circular mantle and the top and bottom facets, which is still much faster than for polyhedrals.

The angular dependency of the scattered energy can be described by the scattering phase function

$$P(\theta) = \frac{1}{2\omega_0}\left[(2\omega_0 - 1)P_{\mathrm{ref}}(\theta) + P_{\mathrm{dif}}(\theta)\right], \tag{1}$$

where $P_{\mathrm{ref}}(\theta)$ denotes the phase function that is due to the reflection or refraction events, $P_{\mathrm{dif}}(\theta)$ accounts for diffraction at the particle projected area, and ω_0 denotes the single scattering albedo. For hexagonal cylinders, diffraction is calculated as described in Ref. 5. For ellipsoidal and circular cylindric particles, one can solve diffraction by assuming an equal-area circular aperture for each particle orientation.

The anisotropy of the scattered radiation can be described by the asymmetry parameter

$$g = \langle \cos\theta \rangle = \int_0^{\pi} P(\theta)\cos\theta \sin\theta \mathrm{d}\theta. \tag{2}$$

Note that the application of the geometrical optics approximation requires locally plane particle surfaces. As the size parameter ($x = 2\pi$ size/wavelength) decreases this condition is increasingly violated near particle edges and for curved particle shapes. For large particles ($x \sim 100$), the contribution of rays scattered near the particle edges is small compared to the total number of scattered rays. According to Ref. 18 the errors in the reflection or refraction processes induced by curvature effects are of the order of λ^2/R^2, i.e., smaller than 0.0005 for the same size parameter, where R denotes the curvature radius.

The present version of the ray-tracing model has been carefully verified by comparing our results with those obtained by exact methods. For spheres at nonabsorbing wavelengths, the agreement in both scattering phase function and polarization pattern was excellent for size parameters above 10,000.

At absorbing wavelengths, the same agreement was found for much smaller size parameters. Furthermore, we performed comparisons for moderately absorbing spheroids and circular cylinders by using the exact **T**-matrix method and also found excellent agreement for size parameters above 60.[19]

The shape of a regular hexagonal cylinder is completely defined by its dimension along the symmetry axis L_h and a characteristic dimension of the hexagonal base facet. The latter is usually defined by the distance $2a_h$ between two opposite points on the hexagon. With regard to axis-equivalent ellipsoids, we define a third value $d = \sqrt{3}/2a$, which is the distance between opposite parallel lines of the hexagon. Thus, the three semiaxes of the axis-equivalent ellipsoid are $(a_e, b_e, c_e) = (L_h/2, \sqrt{3}/2a_h, a_h/2)$. Figure 1 shows a comparison of the shapes of hexagonal particles and axis-equivalent ellipsoids and circular cylinders for the aspect ratios $ar = L_h/(2a_h) = 0.2$, 1, and 5. For a circular cylinder, we use the same dimensions $L_c = L_h$ and $a_c = a_h$ as for the hexagonal cylinder to define the length of the symmetry axis and radius of the circular base facets.

3. Nonabsorbing Particles

In order to study the dependency of light scattering on particle shape only, diffraction and absorption, which depend on size, are excluded in this section. The refractive index is taken to be $n = 1.311 + i0.0$, which corresponds to pure ice at a wavelength of $\lambda = 0.55$ μm.[20] Figure 2 demonstrates the basic differences in the scattering phase function $P_{\text{ref}}(\theta)$ for axis-equivalent hexagonal cylinders, ellipsoids, and circular cylinders. Results are shown for aspect ratios $ar = 0.2$, 1, and 5, i.e., for platelike (or oblate), compact, and columnlike (or prolate) particles. Of course, none of the ellipsoidal shapes can produce the 22° and 46° halos as well as the strong pronounced forward scattering and backscattering, which are characteristic for hexagonal crystals. However, the phase function for circular cylinders as well as for ellipsoids with extreme aspect ratios ($ar = 0.2$, 5) resembles smoothed phase functions of their hexagonal counterparts, especially for oblate ellipsoids. Unlike polyhedral crystals, ellipsoids and circular cylinders exhibit a Mie-type smooth forward scattering caused by the smooth changes in the particles surface curvature. Side scattering is quite similar for ellipsoids with extreme eccentricities and the corresponding hexagonal crystals. On the other hand, differences are largest for $ar = 1$, where the ellipsoid behaves almost like a spherical particle, showing the characteristic weak side scattering and the rainbow maximum in the backscattering region. The scattering maximum at approximately 80° scattering angle for the oblate ellipsoid is a rainbow-type feature as well. This feature shifts toward smaller scattering angles as the aspect ratio departs from 1. Circular cylinders show a 46° halo that is due to minimum deviation at the 90° ice prisms. For $ar = 0.2$ and $ar = 1$, side scattering by circular cylinders is surprisingly similar to that by the hexagonal crystals. For these particle shapes, side scattering is basically determined by external reflections (which have little shape dependency) and by multiple (total) internal reflections from parallel and rectangular facets. Multiple internal reflections within the hexagonal or circular mantle, which are basically the only different ray paths for the two particle types, do not contribute to side scattering. This is not the case for the columnlike cylinders, for which the side scattering by circular cylinders is clearly different from that by hexagonal cylinders. On the other hand, prolate ellipsoids and circular columns behave similarly at a wide range of scattering angles.

None of the ellipsoids and circular cylinders shows the enhanced backscattering at 150° scattering angle, which is characteristic for hexagonal structures. Strikingly, circular and hexagonal cylinders show similar backscattering features at scattering angles ranging from approximately 170° to approximately 180°. This scattering range can be determined by retroreflections at rectangular crystal troughs that both particle types have in approximately equal amounts. Note that direct backscattering is always

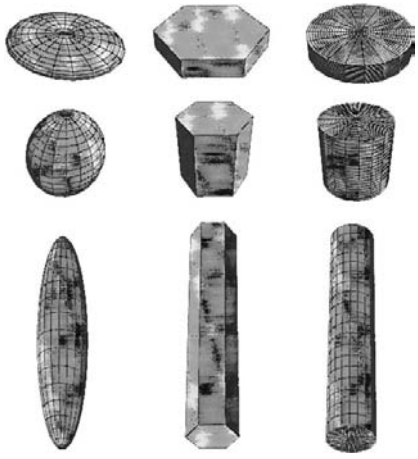

Fig. 1. Particle shapes for axis-equivalent hexagonal crystals, ellipsoids, and circular cylinders with aspect ratios $ar = 0.2$, 1, and 5.

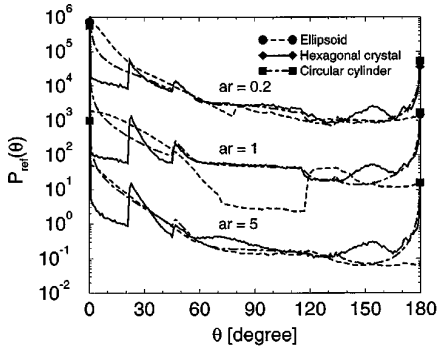

Fig. 2. Ray-tracing phase functions $P_{\text{ref}}(\theta)$ for hexagonal cylinder and axis-equivalent ellipsoids with aspect ratios $ar = 0.2$, 1, and 5. Results for $ar = 0.2$ and $ar = 1$ are multiplied by 10,000 and 100, respectively.

slightly larger for circular than for hexagonal cylinders.

Examining the overall differences in the scattering features, it appears that circular cylinders behave more like hexagonal cylinders than ellipsoids. The reason for this is that both circular and hexagonal cylinders show, contrary to ellipsoids, parallel and rectangular crystal facets.

Figure 3 compares the dependency of the ray-tracing asymmetry parameter g (excluding diffraction) on particle eccentricity ϵ for the particle types discussed above. ϵ is defined as the ratio of the largest to the smallest particle axis. Note that both ellipsoids and circular cylinders generally have larger values for g than their hexagonal counterparts. The oblate particle types are in closer agreement than the prolates. For oblates, the scattering features are basically determined by direct transmissions through (almost) plane-parallel facets that occur with almost the same frequency for circular and hexagonal cylinders. With increasing eccentricity ϵ the g values of the two latter particle types converge to the same value. Differences that are due to the different ray paths at circular and hexagonal mantles vanish as ϵ increases. For oblate ellipsoids there always remains a finite curvature that results in a broader forward scattering behavior, which in turn provides larger asymmetry parameters. The situation is exactly reverse for prolate particles in which, with increasing ϵ, the g values converge for ellipsoids and circular cylinders. For these particle types, scattering can be basically determined by circular and ellipsoidal particle structures that converge more and more as ϵ increases. On the other hand, the hexagonal mantle leads to a noticeably smaller asymmetry parameter. This is due basically to the enhanced backscattering at approximately 150° scattering angle, which is not present for the smooth circular and ellipsoidal particle shapes. Hexagonal and circular cylindric particles provide a monotonously increasing $g(\epsilon)$ curve, whereas ellipsoids show a local minimum at $\epsilon \sim 2.5$ for oblates and $\epsilon \sim 1.5$ for prolates. Apparently, small deviations from the spherical shape ($\epsilon \sim 1$) tend to decrease the asymmetry parameter of ellipsoids. The reason for this is that the rainbow peak broadens and moves toward smaller scattering angles as the eccentricity departs from 1. A further increase in ϵ leads to a stronger forward scattering at particle facets that become more and more plane-parallel and g increases again.

Given these scattering differences between regular hexagonal cylinders, ellipsoids, and circular cylinders, the question arises to what extent deviations from a perfectly hexagonal symmetry lead to better agreement. To answer this question, we consider a statistical distortion of the crystal facets as discussed in Ref. 5. For each reflection or refraction event, the normal vector of the crystal surface is tilted around its original direction. The zenith (azimuth) tilt angle is chosen randomly between $[0, \theta_t^{\max}]$ ($[0, 2\pi]$). The degree of crystal distortion is defined as $t = \theta_t^{\max}/90°$.

Figure 4 shows a comparison of the geometric

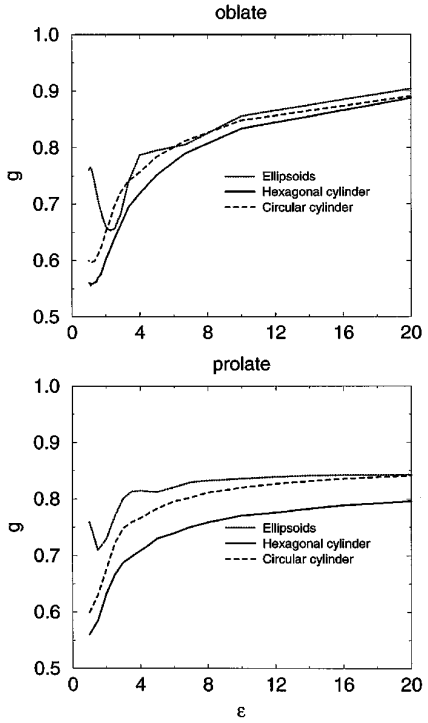

Fig. 3. Asymmetry parameter g for hexagonal and axis-equivalent ellipsoidal particles as a function of particle eccentricity ϵ.

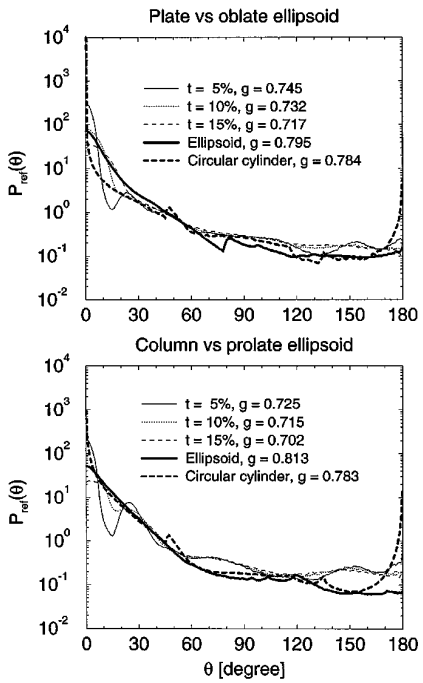

Fig. 4. Scattering phase function $P_{\mathrm{ref}}(\theta)$ (excluding diffraction) for axis-equivalent hexagonal particles—with different degrees of crystal distortion—, ellipsoids, and circular cylinders. Aspect ratio is 0.2 and 5 for prolate and oblate particles, respectively.

scattering phase functions for axis-equivalent distorted hexagonal columns and plates, ellipsoids, and circular cylinders. Generally, increasing distortion leads to better agreement in the forward scattering region. However, differences at side scattering and backscattering essentially remain. For circular versus hexagonal cylinders, differences in the backscattering region even grow. Furthermore, increasing distortion reduces the asymmetry parameter of hexagonal cylinders, i.e., moves it further apart from the value for axis-equivalent ellipsoids and circular cylinders. Altogether, the consideration of possible crystal distortion does not enhance the similarities in the scattering properties of individual particle types.

4. Effects of Absorption

Two wavelengths, $\lambda_1 = 1.6$ μm and $\lambda_2 = 3.7$ μm, are considered here, presenting spectral regions of different absorptivity. The corresponding refractive indices are $n_1 = 1.2895 + i3.53 \times 10^{-4}$ and $n_2 = 1.394 + i6.85 \times 10^{-3}$.[20] Unlike the results in Section 3, the following results include diffraction. Hexagonal particles are defined by their maximum dimension $d_{\max}$, i.e., the length L_h of the columns or the diameter $2a_h$ of the plates. The values chosen for this study are $d_{\max} = 25$, 50, 100, 200, 400, and 800 μm. The aspect ratio for columns and plates are taken from the parameterization by Auer and Veal.[21] In order to minimize differences in the scattering properties of individual particle types that are due to different absorption, ellipsoids and circular cylinders are modified to obey the same effective distance $d_{\text{eff}} = V/C$ as their hexagonal counterparts.[22] Here, V is the particle volume and C is its geometric cross section. One can achieve this modification by multiplying the axes of ellipsoids and circular cylinders by a certain factor. Thus, the axis equivalence, as defined in Section 3, must now be regarded as the axis-ratio equivalence. All the particle dimensions used in this section are listed in Table 1.

For simplicity reasons, we do not provide a discussion of the scattering phase functions for the individual particle types. We just note that the differences and similarities are of the same quality as for a nonabsorbing wavelength (see Figs. 2 and 4), although much smaller in magnitude. The reason for this is that increasing absorption reduces the dependency of light scattering on particle shape, since the scattering properties are more determined by external reflections. For randomly oriented convex particles, light scattering that is due to external reflections is independent of particle shape, contrary to direct transmissions or (multiple) internal reflections.

Figure 5 shows single scattering albedos and asymmetry parameters for the axis/d_{eff}-equivalent hexagonal, ellipsoidal, and circular cylindric particles. First, note that ω_0 for the three particle types does not coincide perfectly. Apparently, a parameter such as effective distance is no guarantee for obtaining the same absorptivities, and shape-dependent differences in the internal ray paths cause different energy attenuations. At both wavelengths, hexagonal columns are stronger absorbers than their smooth-shaped counterparts. For plates, the situation is more or less reverse. However, the differences in ω_0 between the three particle types are rather small at both wavelengths. Thus, we believe that the differences in g versus d_{eff} for individual particle types as shown in the lower diagram of Fig. 5 are basically caused by the different particle shapes rather than by different absorption.

At both wavelengths and for both columnlike and platelike particles, circular cylinders show a more similar $g(d_{\text{eff}})$ curve compared with hexagonal cylinders than ellipsoids. This is especially true at the

Table 1. Dimensions (in micrometers) of the Particles used in Section 4[a]

L_h	r_h	L_c	r_c	a	b	c	d_{eff}	ϵ
Plates								
8.6	12.5	8.1	11.8	4.4	11.2	12.9	9.6	2.9
11.7	25.0	11.1	23.8	6.3	31.0	26.8	15.2	4.3
16.0	50.0	15.5	48.2	9.3	50.6	58.4	23.4	6.2
21.8	100.0	21.2	97.3	13.5	107.2	123.8	34.8	9.2
29.8	200.0	29.2	196.1	19.3	224.9	259.7	50.8	13.4
40.6	400.0	40.0	394.4	27.4	467.3	539.5	72.7	19.7
Columns								
25.0	8.8	22.8	7.8	11.9	7.3	8.4	11.7	1.4
50.0	17.5	44.9	15.7	23.8	14.5	16.7	23.3	1.4
100.0	34.8	89.7	31.2	47.7	28.8	33.2	46.3	1.4
200.0	49.2	177.9	43.8	97.0	41.3	47.7	70.2	2.0
400.0	69.6	353.4	61.5	198.0	59.7	68.9	104.8	2.9
800.0	98.4	703.1	86.5	404.3	86.1	99.5	154.0	4.1

[a] L_h, r_h (L_c, r_c) denote length and hexagon radius of the hexagonal (circular) cylinders. a, b, and c are the ellipsoid semiaxes, and d_{eff} is the effective distance. The dimensionless eccentricity ϵ is also shown.

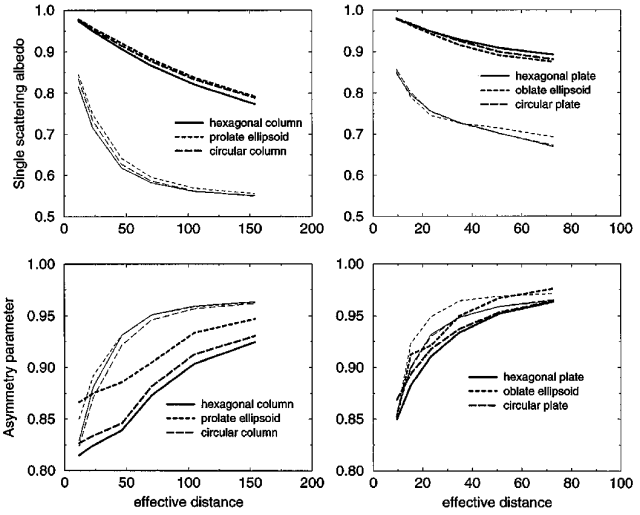

Fig. 5. Single scattering albedo and asymmetry parameter as a function of effective distance for axis/d_{eff} equivalent hexagonal cylinder, ellipsoids, and circular cylinders. Results are shown for $\lambda_1 = 1.6$ μm (thick curves) and $\lambda_1 = 3.7$ μm (thin curves).

stronger absorbing wavelength of λ_2 (thin curves). Note that the asymmetry parameters for hexagonal and circular plates almost perfectly coincide at λ_2, whereas oblate ellipsoids show considerably larger g values here. Given the fact that distortion of hexagonal particles tends to decrease their asymmetry parameter, these differences may get even larger. Thus, in terms of asymmetry parameter, ellipsoids do not seem to qualify as suitable representatives for (absorbing) hexagonal particles. The situation is much better for circular cylinders, which may be regarded as reasonable substitutes, especially for the stronger absorbing wavelength of λ_2.

5. Conclusions

The significant differences in light scattering at hexagonal, ellipsoidal, and circular cylindric particles at a nonabsorbing wavelength ($\lambda = 0.55$ μm) do not suggest the substitution of hexagonal particles by the latter two geometries. The fact that all three particle types exhibit a much larger asymmetry parameter than predicted from flux measurements[11,12] suggests that scattering at regular particle shapes—contrary to randomly shaped particles—is not always representative of real atmospheric ice crystals at nonabsorbing wavelengths.

As a side product it was found that the concept of an effective distance defined by the ratio of the particle volume to its geometric cross section indeed gives fairly good agreement in the single scattering albedos for the three different particle types.

At absorbing wavelengths ($\lambda_1 = 1.6$ μm and $\lambda_2 = 3.7$ μm), the overall differences in the asymmetry parameter between the three particle types are similar to those for the nonabsorbing case but are much smaller in magnitude. In particular, hexagonal and circular plates show strong similarities. The best agreement was found for the stronger absorbing wavelength of λ_2. Although this agreement is due basically to the smaller shape dependency at larger absorption, the remaining shape dependency provides closer agreement between hexagonal and circular cylinders than between hexagonal and ellipsoidal particles. Therefore, if ice crystals happen to be hexagonal in shape, they can be approximated by equivalent circular cylinders at moderately absorbing wavelengths.

This result indicates that **T**-matrix calculations at size parameters below the ray optics regime and at similar or stronger absorbing spectral regions such as the thermal infrared should favor cylindric particle shapes rather than spheroids.

We are grateful to two anonymous referees for their helpful reviews. This research was supported by the NASA First International Satellite Cloud Climatology Project Regional Experiment III project.

References

1. J. I. Peltoniemi, K. Lumme, K. Muinonen, and W. M. Irvine, "Scattering of light by stochastically rough particles," Appl. Opt. **28,** 4088–4095 (1989).
2. A. Macke, "Scattering of light by polyhedral ice crystals," Appl. Opt. **32,** 2780–2788 (1993).
3. Y. Takano and K. N. Liou, "Radiative transfer in cirrus clouds. Part III: Scattering by irregular shaped ice crystals," J. Atmos. Sci. **52,** 818–837 (1995).
4. J. Iaquinta, H. Isaka, and P. Personne, "Scattering phase function of bullet rosette ice crystals," J. Atmos. Sci. **52,** 1401–1413 (1995).
5. A. Macke, J. Mueller, and E. Raschke, "Single scattering properties of atmospheric ice crystals," J. Atmos. Sci. (1996), in press.
6. A. J. Heymsfield and C. M. R. Platt, "A parameterization of the particle size spectrum of ice clouds in terms of the ambient temperature and the ice water content," J. Atmos. Sci. **41,** 846–855 (1984).
7. J. Hallet, "Faceted snow crystals," J. Opt. Soc. Am. A **4,** 581–588 (1987).
8. B. J. Mason, "Snow crystals, natural and man-made," Contemp. Phys. **33,** 227–243 (1992).
9. P. N. Francis, "Some aircraft observations of the scattering properties of ice crystals," J. Atmos. Sci. **52,** 1142–1154 (1995).
10. J.-F. Gayet, O. Crepel, and J.-F. Fournol, "A new polar nephelometer for *in situ* measurements of microphysical and optical properties of clouds," in *Proceedings of the American Meteorological Society Conference on Cloud Physics* (American Meteorological Society, Dallas, Tex., 1995), pp. 26–30.
11. G. L. Stephens, S-C. Tsay, P. W. Stackhouse, and P. J. Flatau, "The relevance of the microphysical and radiative properties of cirrus clouds to climate and climatic feedback," J. Atmos. Sci. **47,** 1742–1753 (1990).
12. S. Kinne, T. A. Ackermann, A. J. Heymsfield, F. P. J. Valero, K. Sassen, and J. Spinhirne, "Cirrus microphysics and radiative transfer: cloud field study on 28 October 1986," Mon. Weather Rev. **120,** 661–684 (1992).
13. P. C. Waterman, "Symmetry, unitarity, and geometry in electromagnetic scattering," Phys. Rev. D **3,** 825–839 (1971).
14. M. I. Mishchenko, "Light scattering by size-shape distribution of randomly oriented axially symmetric particles of a size comparable to a wavelength," Appl. Opt. **32,** 4652–4666 (1993).
15. M. I. Mishchenko, "T-matrix computations of light scattering by large spheroidal particles," Opt. Commun. **109,** 16–21 (1994).
16. J. E. Hansen, "Multiple scattering of polarized light in planetary atmospheres. Part II. Sunlight reflected by terrestrial water clouds," J. Atmos. Sci. **28,** 1400–1426 (1971).
17. M. I. Mishchenko and L. D. Travis, "Light scattering by polydisperse, rotationally symmetric nonspherical particles: linear polarization," J. Quant. Spectrosc. Radiat. Transfer **51,** 759–778 (1994).
18. P. Beckmann, *The Depolarization of Electromagnetic Waves* (Golem Press, Boulder, Colo., 1968).
19. A. Macke, M. I. Mishchenko, K. Muinonen, and B. E. Carlson, "Scattering of light by large nonspherical particles: ray optics approximation versus T-matrix method," Opt. Lett. **20,** 1934–1936 (1995).
20. S. G. Warren, "Optical constants of ice from the ultraviolet to the microwave," Appl. Opt. **23,** 1206–1225 (1984).
21. A. H. Auer and D. L. Veal, "The dimensions of ice crystals in natural clouds," J. Atmos. Sci. **27,** 919–926 (1970).
22. D. L. Mitchell and W. P. Arnott, "A model predicting the evolution of ice particle size spectra and radiative properties of cirrus clouds. Part II: Dependence of absorption and extinction on ice crystal morphology," J. Atmos. Sci. **51,** 817–832 (1994).